Experimental Realization of a Circuit-Based Broadband Illusion-Optics Analogue

Chao Li,[1] Xiankun Meng,[1] Xiao Liu,[1] Fang Li,[1] Guangyou Fang,[1] Huanyang Chen,[2,*] and C. T. Chan[3]

[1]*Key Laboratory of Microwave and Electromagnetic Radiation, Institute of Electronics, Chinese Academy of Sciences (IECAS), 100190 Beijing, China*

[2]*School of Physical Science and Technology, Soochow University, Suzhou, Jiangsu 215006, China*

[3]*Department of Physics and William Mong Institute of Nano Science and Technology, Hong Kong University of Science and Technology, Clear Water Bay, Hong Kong, China*

(Received 19 May 2010; revised manuscript received 8 November 2010; published 2 December 2010)

We experimentally demonstrate the first metamaterial ''illusion optics'' device—an ''invisible gateway'' by using a transmission-line medium. The device contains an open channel that can block waves at a particular frequency range. We also demonstrate that such a device can work in a broad frequency range.

DOI: 10.1103/PhysRevLett.105.233906 PACS numbers: 41.20.Jb, 42.79.−e

Transformation optics [1–3] has paved the way for the rational design of interesting wave manipulation conceptual devices [4–14]. Recently, the combination of the complementary media concept [15] with the transformation optics technique [16] has motivated a series of illusion optics devices [17–20], which can create optical illusions. However, such effects are limited to theoretical analysis and numerical simulations. Using a transmission-line medium, we realized the first experimental demonstration of a two dimensional illusion optics device, an ''invisible gateway'' [21,22], which is an open channel that appears to be blocked for waves of a selected range of frequencies. We also measured the performance of the device and demonstrated its broadband functionality.

To start with, let us consider a configuration that is illustrated schematically in Fig. 1. A perfect electric conductor [PEC, marked by blue (darker gray) color] wall partitions space [air, $\epsilon = \mu = 1$, denoted by green (gray) color] into two domains. A channel is then opened in the PEC wall with a double negative material (DNM, $\epsilon' = \mu' = -1$) filled inside the trapezoidal region [marked by red (darkest gray) color] and an air channel. From the viewpoint of transformation optics [22], the DNM will project the PEC boundary adjacent to it into another optically equivalent PEC boundary (marked by the dashed line) so that the wall with an air channel will look like a continuous PEC wall for the observers outside at the designed frequency. Such an air channel was also called an ''invisible gateway'', meaning that an observer cannot ''see'' the open channel, but would rather see some reflection leading to the illusion that the channel is blocked. For the lack of a better term to describe the system, we will use ''invisible gateway'' hereafter. Electromagnetic (EM) wave incident from one side of the wall cannot reach to another side while other entities are allowed to pass through the open channel. However, it is challenging to implement such a device electromagnetically due to the difficulty in realizing the perfect lens [23]. It should be noted that, such an invisible gateway can be applied to both two dimensional (2D) and three dimensional (3D) geometries. In this Letter, we will only focus on the 2D case.

Materials with specific permittivity and permeability tensors can be mimicked by periodic TL networks to give similar propagation behaviors. The TL versions of conventional double negative materials (DPMs) and artificial double negative materials (DNMs) have been investigated previously [24] and demonstrated experimentally to have the focusing effect that overcomes the classical diffraction limit [25].

Here, we choose a periodic inductor-capacitor (L-C) network to mimic the configuration depicted in Fig. 1. The unit cell to mimic the air region is shown in Fig. 2(a), where the series inductor and shunt capacitors can act as an isotropic medium with positive equal permittivity and permeability. The DNM is mimicked by the dual L-C configuration as shown in Fig. 2(b), where the position of L and C are interchanged. There is a mapping between the L-C network equations and the polarized transverse electric (or magnetic) Maxwell's equations with voltages V

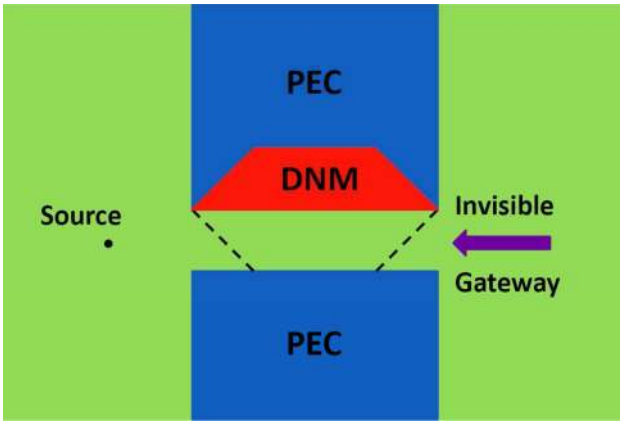

FIG. 1 (color online). Schematic picture of an electromagnetic invisible gateway. The air, PEC wall and DNM are denoted by green (gray), blue (darker gray) and red (darkest gray) colors, respectively.

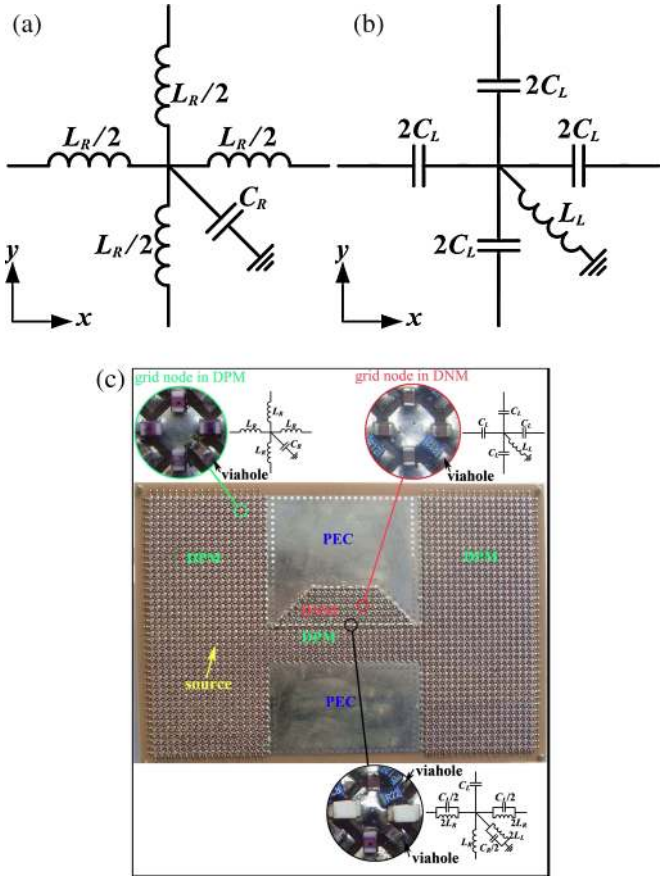

FIG. 2 (color online). Unit cells of periodic L-C structures to mimic the DPMs (a) and DNMs (b), and the real experimental device (c).

and currents I mapped to the field quantities E and H. In the long-wavelength limit, the dimension of the unit cell Δ is much smaller than the wavelength, therefore the relationship between the circuit parameters (the capacitance and inductance in the network) and the materials parameters (the effective permittivity and permeability) can be derived as [26],

$$\epsilon_R = \frac{C_R}{\Delta}, \qquad \mu_R = \frac{L_R}{\Delta}, \tag{1}$$

$$\epsilon_L = -\frac{1}{\omega^2 L_L \Delta}, \qquad \mu_L = -\frac{1}{\omega^2 C_L \Delta}, \tag{2}$$

where Δ is the length of the unit cell in the x and y direction, and the subscripts "R" and "L" refer to the case of mimicking a DPM and DNM, respectively.

In order to mimic the invisible gateway device in Fig. 1, two requirements should be met at the design frequency. One is that both the DPM and DNM network must behave like effective media with $\sqrt{\mu_R \epsilon_R} f \Delta \leq 1$ and $\sqrt{\mu_L \epsilon_L} f \Delta \leq 1$. The other is $\epsilon_L = -\epsilon_R$ and $\mu_L = -\mu_R$. Here we choose the unit cell parameters as $\Delta = 6$ mm, $L_R = 47$ nH, $C_R = 82pF$ to meet all the above requirements in a design frequency $f_0 = 51$ MHz. These parameters result in an effective wavelength of 60 mm. The experimental device [Fig. 2(c)] is fabricated on a grounded flame retardant 4 (FR4) substrate of thickness 1 mm and dielectric constant $\epsilon_r = 4.3$. The whole structure has 61 grid nodes in the x direction and 41 grids in y direction. The distance between two adjacent nodes is $\Delta = 6$ mm (i.e., 0.1λ). The structure measures totally about 390 mm $\times$ 270 mm. The magnified views of the grid nodes are also shown in the insets of the Fig. 2(c). The nodes in the DPM region consist of four surface-mounted inductors in series and one capacitor in shunt to the ground by a via-hole (see schematic plot in Fig. 2(a)]. The left-handed unit cell consists of four surface-mounted capacitors in series and one inductor in shunt to the ground by a via-hole [see the schematic plot in Fig. 2(b)]. Grounded PEC plates are used to mimic the PEC walls in Fig. 1. In our design, the outer boundaries of the DPM regions are truncated by being connected with Bloch impedances [27] which are applied to achieve matching absorption to mimic the infinitely extended background. A topology which is very similar to the Yee grids in the finite-difference time-domain (FDTD) method is employed at the interface of the DPM region and its complementary counterpart [28]. As shown in the lower inset of Fig. 2(c), the series branches of the node consists of the parallel connection of $2L_R$ and $C_L/2$, while the shunt branch consists of the parallel connection of $C_R/2$ and $2L_L$. With such a topology, a more precise equivalence to the continuity condition of tangential electric and magnetic field at the interface between two different medium can be achieved.

Before performing the experiment, we have simulated the expected performance of the device using Agilent's Advanced Design System (ADS). In the simulation, a 1 A current source is connected between the center of the node (11, 18) and the ground to generate a point source excitation. The simulated result for an ideal lossless case at the design frequency is shown in Fig. 3(a). Strong surface waves can be observed at the interface of the DPM and

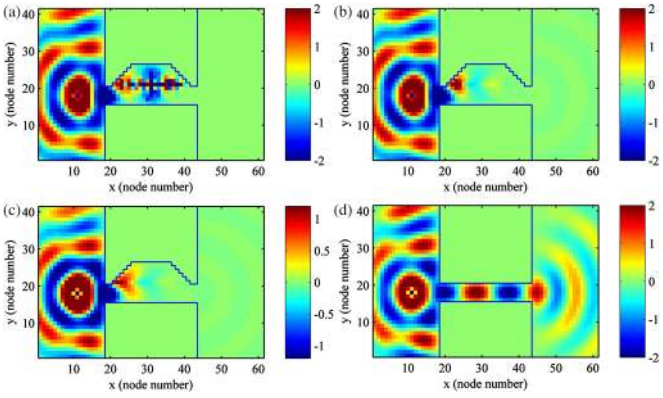

FIG. 3 (color online). Simulated node voltage distribution. Invisible gateway with DNM for lossless case (a), of very little loss case ($Q = 10^5$, (b), $Q = 10$ case (c); with PEC instead of DNM (d).

DNM and the waves from the point source are completely blocked from propagating to the right domain. When a small loss is introduced (the quality factor for all the inductors and capacitors is set to be $Q = 10^5$), the surface waves are partially damped, as shown in Fig. 3(b). However, the field in the right domain is still very weak which means that most of the waves excited by the source in the left domain are mostly blocked by the gateway device. This phenomenon can also be observed when Q is set to be 10 as another example, as shown in Fig. 3(c). This means that the invisible gateway is robust against material loss, which is inevitable in experiments. For comparison, Fig. 3(d) shows the simulated voltage distribution when the DNM in the trapezoidal region is replaced by PEC. In this case, the waves can evidently propagate to the right domain.

In the experiments, an Agilent E5071C vector network analyzer (VNA) was employed to measure the transmission coefficient, which is in proportional to the voltage of the grid nodes. Port 1 of the VNA provides the excitation via a coaxial feed, with its outer conductor mounted onto the ground plane at the backside of the FR4 substrate, and its center pin extending through a hole in the substrate and soldered to the center of the node (11, 18), which is same as that in the simulation. Hence, a point source is introduced. Port2 of the VNA provides a near-field coaxial probe that can scan over the surface of the whole structure. To ensure the precision of the measurement, the disturbance of the voltage distribution as the detecting probe touching the node must be well controlled [29]. Here, a broadband amplifier with very high input impedance is designed and inserted between the detecting probe and Port2 of the VNA. The amplifier is designed based on the topology of differential amplifier with current feedback. The measured input impedance is more than $2k$ Ohms and the measured voltage gain is 20 dB $\pm$ 0.2 dB over the frequency band from dc to 100 MHz. We note that in the experiment, the value of the excitation current at node (11, 18) varies as frequency changes, due to the frequency-dependent input impedance at that node resulting from the dispersion of the whole network, while in the ADS simulation, the source has fixed current amplitude for all the frequencies. In order to conduct a reasonable comparison of the wideband property, the experimental excitation currents at each frequency were extracted by applying Kirchhoff's current laws at node (11, 18), and then the experimental results are normalized to 1 A excitation current to keep consistence with simulation.

The measured results at the design frequency $f =$ 51 MHz is shown in Fig. 4(a). For comparison, Fig. 4(d) shows the measured voltage distribution when the DNM is replaced by the PEC. These two results are very similar to the numerical simulations shown in Figs. 3(c) and 3(d), which verifies that our device has the realistic illusion property of the invisible gateway. In the frequency band around 51 MHz (the designed frequency), the chip inductors and capacitors have nonresonant nature and the values of L_R, L_L and C_R, C_L change gradually when the frequency changes. Although the requirement of the complementary medium condition is only satisfied strictly at the designed frequency, the "optical cancellation" property still remains effective even if the material properties are slightly off. The reasonably wide functional bandwidth is evident in Figs. 4 and 5 [30]. Figs. 4(b) and 4(c) show the functionalities of the device with DNM at frequencies 46 and 56 MHz, while Figs. 4(e) and 4(f) show the functionalities of the device with PEC instead of DNM at frequencies 46 and 56 MHz. The illusion property clearly extends to such frequencies. To quantitatively evaluate the bandwidth of our device, we calculated the power leaked into the right domain for the case with DNMs, P_{DNM} and with PECs instead of DNMs, P_{PEC} based on $P = \sum_i V(i) \cdot I^*_{\mathrm{out}}(i)$, where $V(i)$ and $I_{\mathrm{out}}(i)$ are the node voltages and outward currents on the nodes along the right window of the gateway. The leaked power (P_{DNM} and P_{PEC}) are plotted in a log scale (decibel milliWatt—dBm) in Fig. 5(a) as a function of frequencies. The (red) solid line shows the experimental results with DNM, while the (green) dotted dashed line shows the corresponding ADS simulation with a quality factor $Q = 10$ for comparison. The (blue) dashed line shows the experimental results with DNM replaced by PEC, while the (black) dotted line denotes the corresponding ADS simulation results. We note the qualitative agreement between the simulation and the experiment. From Fig. 5(a), we see that the illusion

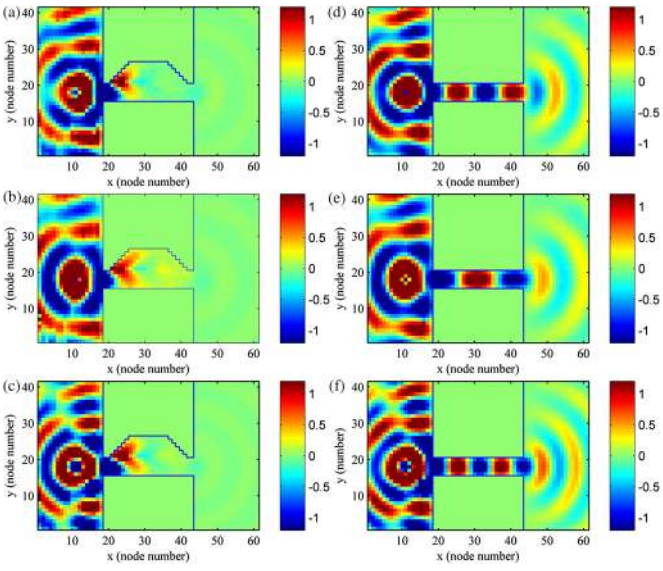

FIG. 4 (color online). Measured node voltage distribution (normalized to 1 A excitation current). Gateway with DNM at the trapezoidal region at frequencies $f = 51$ MHz (a), 46 MHz (b), and 56 MHz (c); Gateway with DNM replaced by PEC at frequencies $f = 51$ MHz (d), 46 MHz (e), and 56 MHz (f). The complete node voltage data sets can also be found in Ref. [30].

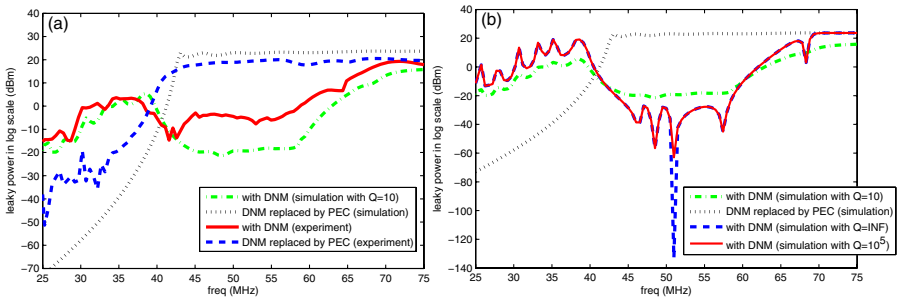

FIG. 5 (color online). The leaked power from the left domain for the cases of PEC and DNMs with various Q factors. The (black) dotted lines in both (a) and (b) denote the simulation results with DNM replaced by PEC. The (green) dotted dashed lines in both (a) and (b) denote the simulation results for DNM with a quality factor $Q = 10$. The (red) solid line in (a) denotes the experimental results with DNM, while the (blue) dashed line in (a) denotes the experimental results with DNM replaced by PEC. The (red) solid line in (b) denotes the simulation results for DNM with a quality factor $Q = 10^5$, while the (blue) dashed line in (b) denotes that the lossless case.

device transmits much less power than the control device at about 45 MHz to 60 MHz. For the frequencies below 40 MHz, the absolute value of the refractive index of DNM is no longer equal to or close to -1. When the frequency is lower than the designed frequency, the DNM media becomes a double negative media with a higher absolute value of refractive index, and it is does not reject the EM wave. The channel thus becomes effectively wider, and the cutoff frequency moves to a lower frequency. Therefore there is no "optical cancelling" effect due to complementary media in the range below 40 MHz. It is only near the design frequency that the complementary media cancellation shuts off the channel, leading to a dip in the range of about 45 to 60 MHz, which can be regarded as the working frequencies of our invisible gateway. Figure 5(b) shows simulated leaked power for cases with various Q factors. The (black) dotted line shows the simulation results with DNM replaced by PEC, while the (green) dotted dashed line denotes the ADS simulation for DNM with a quality factor $Q = 10$ [Same to Fig. 5(a)]. The (red) solid line now shows the ADS simulation for DNM with a quality factor $Q = 10^5$, while the (blue) dashed line now shows the ADS simulation for DNM with an infinite quality factor (lossless case). The broadband functionality is quite robust for various Q factors.

To summarize, we fabricated a device to mimic an electromagnetic invisible gateway. The simulation and measurement results confirm its functionalities. In addition, such a device works for a rather broadband. Other metamaterial illusion optical devices (such as an external cloak) can also be designed and emulated by using the similar transmission-line medium.

This work was supported by the National Natural Science Foundation of China (60990323, 60990320, and 11004147), the Knowledge Innovation Program of Chinese Academy of Sciences, the Natural Science Foundation of Jiangsu Province under Grant No. BK2010211, and Hong Kong RGC grant 600209. Computation resources at Hong Kong were supported by the Shun Hing Education and Charity Fund.

*kenyon@ust.hk

[1] U. Leonhardt, Science **312**, 1777 (2006).
[2] J. B. Pendry, D. Schurig, and D. R. Smith, Science **312**, 1780 (2006).
[3] H. Y. Chen, C. T. Chan, and P. Sheng, Nature Mater. **9**, 387 (2010).
[4] H. Y. Chen *et al.*, Phys. Rev. Lett. **102**, 183903 (2009).
[5] Y. G. Ma *et al.*, Nature Mater. **8**, 639 (2009).
[6] N. Kundtz and D. R. Smith, Nature Mater. **9**, 129 (2010).
[7] D. Schurig *et al.*, Science **314**, 977 (2006).
[8] R. Liu *et al.*, Science **323**, 366 (2009).
[9] S. Tretyakov *et al.*, Phys. Rev. Lett. **103**, 103905 (2009).
[10] J. Valentine *et al.*, Nature Mater. **8**, 568 (2009).
[11] L. H. Gabrielli *et al.*, Nat. Photon. **3**, 461 (2009).
[12] I. I. Smolyaninov *et al.*, Phys. Rev. Lett. **102**, 213901 (2009).
[13] X. Liu *et al.*, Appl. Phys. Lett. **95**, 191107 (2009).
[14] C. Li, X. Liu, and F. Li, Phys. Rev. B **81**, 115133 (2010).
[15] J. B. Pendry and S. A. Ramakrishna, J. Phys. Condens. Matter **15**, 6345 (2003).
[16] U. Leonhardt and T. G. Philbin, New J. Phys. **8**, 247 (2006).
[17] T. Yang *et al.*, Opt. Express **16**, 18545 (2008).
[18] J. Ng, H. Y. Chen, and C. T. Chan, Opt. Lett. **34**, 644 (2009).
[19] Y. Lai *et al.*, Phys. Rev. Lett. **102**, 093901 (2009).
[20] Y. Lai *et al.*, Phys. Rev. Lett. **102**, 253902 (2009).
[21] X. Luo *et al.*, Appl. Phys. Lett. **94**, 223513 (2009).
[22] H. Y. Chen *et al.*, New J. Phys. **11**, 083012 (2009).
[23] J. B. Pendry, Phys. Rev. Lett. **85**, 3966 (2000).
[24] G. V. Eleftheriades, A. K. Iyer, and P. C. Kremer, IEEE Trans. Microwave Theory Tech. **50**, 2702 (2002).
[25] A. Grbic and G. V. Eleftheriades, Phys. Rev. Lett. **92**, 117403 (2004).
[26] C. Caloz and T. Itoh, IEEE Trans. Antennas Propag. **52**, 1159 (2004).
[27] A. Grbic and G. V. Eleftheriades, IEEE Trans. Antennas Propag. **51**, 2604 (2003).
[28] A. Taflove and S. C. Hagness, *Computational Electrodynamics: The Finite-Difference Time-Domain Method* (Artech House, Norwood, MA, 2005), 3rd ed.
[29] G. Palumbo and S. Pennisi, *Feedback Amplifiers: Theory and Design* (Kluwer Academic Publishers, Dordrecht, The Netherlands, 2002).
[30] See supplementary material at http://link.aps.org/supplemental/10.1103/PhysRevLett.105.233906.